Chemical Science

ROYAL SOCIETY OF CHEMISTRY

EDGE ARTICLE

View Article Online
View Journal | View Issue

Cite this: *Chem. Sci.*, 2021, **12**, 1778

All publication charges for this article have been paid for by the Royal Society of Chemistry

Received 15th September 2020
Accepted 30th November 2020

DOI: 10.1039/d0sc05100d

rsc.li/chemical-science

Two helices from one chiral centre – self organization of disc shaped chiral nanoparticles†

Huanan Yu,[a] Wentao Qu,[b] Feng Liu[b] and Georg H. Mehl*[ab]

Gold nanoparticles (AuNPs) have been prepared and surface-functionalized with a mixture of 1-hexanethiol co-ligands and chiral discogen ligands separated from a disulfide function *via* a flexible spacer. Polarized optical microscopy together with differential scanning calorimetry showed that the organic corona of the nanocomposite forms a stable chiral discotic nematic (N_D^*) phase with a wide thermal range. Synchrotron X-ray diffraction showed that gold NPs form a superlattice with *p*2 plane symmetry. Analysis indicated that the organic corona takes up the shape of a flexible macrodisk. Synchrotron radiation-based circular dichroism signals of thin films are significantly enhanced on the isotropic-LC transition, in line with the formation of a chiral nematic phase of the organic corona. At lower temperatures the appearance of CD signals at longer wavelengths is associated with the chiral organisation of the NPs and is indicative of the formation of a second helical structure. The decreased volume required and the chiral environment of the disc ligands drives the nanoparticles into columns that arrange helically, parallel to the shortest axis of the two dimensional lattice.

The exploration of chiral nanomaterials is a rapidly evolving fascinating field with uses ranging from catalysis, chiral molecular sensing, stereoselective separations to super-resolution imaging.[1–3] Bottom-up approach design strategies for nanoparticles (NPs) or nanorods (NRs) as composites in liquid crystal (LC) matrices have been developed, making use of progress in synthesis strategies and characterization techniques.[4–6] For optical applications symmetry breaking by introducing chirality into the systems at the nanoscale is critical.[7] So far, efforts to obtain chiroptical NP-LC systems have relied mainly on NPs doped in LC hosts: either chiral nematic templates disperse NPs into chiral assemblies[8] or the NPs functionalized with chiral ligands are included in achiral nematic LCs;[9] both strategies aim to transfer and amplify chiral effects.[10,11] Beyond the scientific challenge of generating nanocomposites where the interplay of bottom-up structuring enables plasmonic interactions of the NPs, leading to novel, so called metamaterials properties, there are new uses ranging from novel display devices,[12] to more advanced optical communications using spin information between LEDs[13] and in quantum teleportation for optical computing.[14]

Precise size control of NPs in LC matrices in combined systems has been found critical to avoid phase separation or precipitation of NPs.[15] For intrinsic liquid crystalline NP-LC systems, targeting of the LC phase range to be close to ambient is of utmost importance, as delamination of ligands occurs at elevated temperatures, even for very stable thiol functions. Degradation tends to occur above 100 °C.[16] Inclusion of chiral groups in the organic corona can lead to chiral LC phase behavior, but there is little evidence that the NPs experience a chiral distortion in their packing; experimental evidence indicates that the nanocomposites minimize energy by packing in non-chiral superlattices and chirality is confined to the corona.[17]

Here we show that a combination of small NPs with a carefully designed chiral organic coating results in chiral assembly behaviour of both the NPs and the organic corona. Our approach is strictly modular. The surface of the gold NPs is covered and passivated by hexylthiol groups and chiral lipoic acid derivates bearing *via* a spacer the mesogenic groups. We

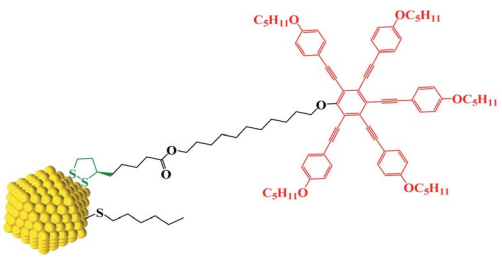

Chart 1 Sketch of the functionalized gold nanoparticle system AuDLC*.

[a]*Department of Chemistry, University of Hull, Hull, HU6 7RX, UK*
[b]*State Key Laboratory for Mechanical Behaviour of Materials, Shaanxi International Research Centre for Soft Matter, Xi'an Jiaotong University, Xi'an, P. R. China. E-mail: g.h.mehl@hull.ac.uk*

† Electronic supplementary information (ESI) available. See DOI: 10.1039/d0sc05100d

note that lipoic acid, a naturally occurring chiral antioxidant explored elsewhere for the treatment of several diseases, is bound with a dithiolate bridge *via* two atoms to the Au surface (see Chart 1).[18] This places the chiral moiety rigidly in position onto the NPs, making thus a chiral surface.[19] A pentaalkynylbenzene (PA) derivative was selected as mesogenic group, as this structural motif is known to promote reliably discotic nematic phase (N_D) behaviour.[20] The much larger volume of the PA group, when compared to typical rod shaped mesogens, whilst also delivering LC behaviour close to ambient, is anticipated to impact more strongly on the spatial organization of neighbouring NPs when compared to calamitic functionalized NP systems.[17] The formation of helically ordered superstructures is studied by a combination of dedicated thin film optical polarizing microscopy, X-ray diffraction and synchrotron radiation-based circular dichroism (SRCD). A structural model is proposed based on a chiral nematic phase made up of AuNPs coated with chiral shells forming flexible macrodisks which in turn assemble in a superlattice.[21–23]

The design, synthesis and chemical characterization of the chiral discogen is described in the ESI.† The precursor disk-like mesogen which forms exclusively a N_D phase above 100 °C consists of six aromatic rings flanked by flexible pentyloxy chains and an undecyloxy chain bearing a terminal hydroxy group (Fig. S1†). The attachment of the flexible (*R*)-(+)-1,2-dithiolane-3-pentanoic tail was predicted to promote the desired N_D^* phase. The new target discogen was obtained in a high yield (93.1%) reaction. For the synthesis and purification of LC-functionalized AuNPs, denoted as AuDLC*, a synthetic pathway was developed involving first the preparing and purifying of the alkylthiol coated NPs to which LC groups are linked, using an exchange reaction (for details see the Scheme 1 in ESI†).[24,25]

The thermal behaviour of the chiral discogen was examined by differential scanning calorimetry (DSC) and polarized optical microscopy (POM). The target discogen shows clearly a chiral nematic phase with the characteristic bundles of oily streaks (Fig. S2†). On heating (Fig. S3†), N_D^* phase formation was observed at 49.0 °C from the crystalline state, with the material turning into an isotropic liquid at 95.7 °C ($\Delta H = 0.20$ J g^{-1} or 0.28 kJ mol^{-1}). Formation of the mesophase from the isotropic state on cooling started from 94.5 °C with an enthalpy change of 0.12 J g^{-1} (0.17 kJ mol^{-1}), followed by a slow crystallisation occurring at 5.1 °C. In brief, the chiral phase behaviour of the target ligand is exclusively chiral nematic, enantiotropic and with a wide thermal range of up to 89.4 °C.

The ^{1}H-NMR spectra of the investigated AuDLC* nanocomposite and the comparison with the spectra of the monomer ligand (Fig. S4†) indicate that the chiral discogen with the disulfide group are chemically attached onto the surface of AuNPs with high efficiency. A typical feature for such NPs are the broadened ^{1}H-NMR spectra caused by the reduced mobility of alkyl chains of the ligands when anchored to NPs and additionally the sharp peaks present in the free ligand have disappeared, typical for such systems.[26] The absence of mobile free discogen using thin layer chromatography (silica, with dichloromethane as mobile phase) confirms this result. The amount of chiral discogen bounded onto the gold surface relative to the number of 1-hexanethiol groups was determined from the ^{1}H-NMR spectra of AuDLC*. The ratio of hydrocarbons to discogens was found to be 2 : 3. Transmission Electron Microscopy (TEM) investigations confirm that this sequential synthesis affords nanoparticles of low polydispersity (Fig. 1a); the average particle size is ~2.5 ± 0.5 nm. Thermo-gravimetric analysis (TGA) was performed (Fig. S6†) and gives the weight fraction of gold in AuDLC* to be 47.8% (wt/wt). The mesogen density per Au NP was calculated (ESI† Part 7) by combining the ^{1}H-NMR results (Fig. S4†) with the model developed by Gelbart *et al.*[27] On the basis of these data, we obtain that there are on average 211 Au atoms per particle, and a total number of 53 ligands per particle, of which 32 are chiral discogens and 21 are hexylthiol groups (Table S1†). This is in accord with a ligand density of up to ~6.3 ligands per nm^2.[28] Additionally, the characteristic peaks in the UV-vis spectra of AuDLC* arise from the combination of gold (~500 nm) and LC ligands (absorption maxima at 238, 261 and 351 nm with two shoulder peaks at 378 and 421 nm) (Fig. S7†).

The mesophase behaviour of the AuDLC* nanocomposite was first characterized by POM observation. As shown in Fig. 1b and c, upon cooling from the isotropic liquid, the colour in the POM texture changes from light green to yellow and we

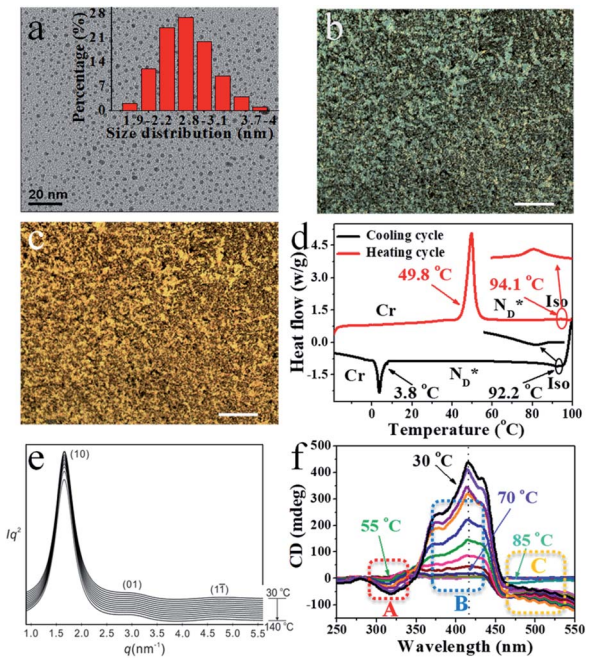

Fig. 1 (a) TEM image of 2.5 nm AuDLC* nanocomposite (inset: the size distribution of AuDLC*). POM micrographs of AuDLC* (b) 86.5 °C (90° crossed polarizer) (×100 μm). (c) 37.8 °C (90° crossed polarizer) (×100 μm). (d) DSC of AuDLC* at heating and cooling rate of 10.0 °C min^{-1} (e) SAXS diffractograms of AuDLC* on heating from 30 °C to 140 °C. (f) SRCD spectra of sheared AuDLC*. Recorded in 5 °C steps on cooling from 100 °C to 30 °C. The enlarged plots in dotted regions A–C are shown in Fig. S12b–d.† The CD intensities at a selected wavelengths in each region (A, B and C) are plotted as a function of temperature in Fig. S13† and these plots clearly show the difference in the formation process between the two helical structures.

Table 1 Transition temperatures (°C) of free chiral discogen and AuDLC*, as determined by DSC (second cooling at rate of 10.0 °C min^{-1})[a]

Compound		Transition temperature/°C (enthalpy)			
Monomer	Iso	94.5 (0.12 J g^{-1} or 0.17 kJ mol^{-1})	N_D^*	5.1	Cr
AuDLC*	Iso	92.2 (0.043 J g^{-1} or 0.12 kJ mol^{-1})	N_D^*	3.8	T_g

[a] Iso = isotropic, Cr = crystalline, Tg = glass transition, N_D^* = chiral discotic nematic phase.

associate this with the helical pitch in AuDLC* increasing with decreasing temperature. In some regions of the POM slides, a chiral nematic phase with the typical Grandjean texture (Fig. S8a and b†) is found. The LC textures in AuDLC* do recover after gently pressing the microscope coverslip indicating that the LC-decorated NPs form a stable N_D^* phase and birefringent textures remain stable at ambient (Fig. S9†). DSC investigations (Fig. 1d) confirm that the AuDLC* nanocomposite shows a thermodynamically stable (enantiotropic) mesophase. In DSC experiments on cooling a small peak associated with the isotropic to N_D^* phase transition (92.2 °C) can be detected, and at a low temperature (3.8 °C), the glass transition occurs. The transition peak for the N_D^*-iso transition is wider than in the pure chiral discogen, typical for such systems.[4] This is associated with the reduced mobility of the LC groups attached to the NPs. The thermal transitions determined by DSC for the pure chiral discogen and AuDLC* are collected in Table 1, showing the low values typical for iso-N_D^* transitions.[20] In contrast to the free chiral ligand, the NPs coated with the chiral ligand and hexylthiol groups show a small decrease in transition temperatures. This could be attributed to both the plastifying effects of the hexylthiol co-ligands and packing constraints of the LC groups due to the attachment to the NPs. This view is supported by the DSC data for the iso-N_D^* transition at 0.043 J g^{-1} (0.12 kJ mol^{-1}, considering the evaluated 32 chiral discogen ligands per particle).

In synchrotron XRD studies of the AuDLC* nanocomposite, three peaks are obtained in the small angle regions (Fig. 1e) with values of q: 2.0160, 3.3289 and 4.9015 nm^{-1}; equivalent to values of 3.12 nm, 1.89 nm and 1.28 nm (Table S2†). The peaks could be indexed as (10), (01) and (1$\bar{1}$) reflections of a columnar lattice with a $p2$ plane group (Fig. 2a). The unit cell parameters are a = 4.17 nm, b = 2.52 nm and $\gamma \sim 48.4°$. When comparing the estimated average volume, the area of the lattice is 10.51 nm^2. On cooling from the isotropic to room temperature, a slight increase of the lattice parameters by 2–3% (~0.1 nm) is noticeable and γ decreases from 48.4° to 46.2° at ambient (Fig. S10†). The increase of a and b at lower temperatures is concomitant with shrinking of the NP corona in the third dimension, considering the volume reduction of organics with decreasing temperature. The superlattice is stable beyond the stability of the LC phase, indicating that overall the shape of the organic corona is maintained over the chemical stability region of the materials. Using the lattice

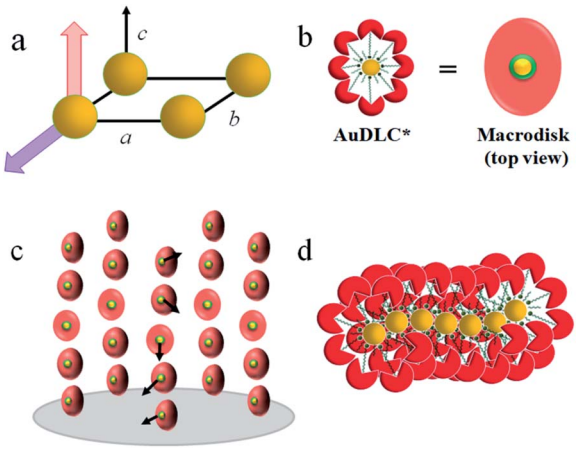

Fig. 2 Schematic representation of (a) $p2$ lattice with parameters a = 4.17 nm, b = 2.52 nm and the angle γ ~48.4°; spatial direction c not defined by the lattice. Red arrow: N_D^* helix axis; purple arrow: plasmonic interactions. (b) AuDLC* macrodisk. Yellow: gold core; red: PA unit; green: chiral sheath. (c) N_D^* phase formed by functionalized NPs. (d) Chiral assembly behaviour of gold NPs along the axis of smallest lattice parameter b.

area of 10.51 nm^2 and the calculated average volume of an AuDLC* particle of 64.30 nm^3, the value of 6.12 nm in the third dimension, likely the main axis of the orientationally ordered mesogens is needed to account for the total volume. This value is somewhat shorter than the estimated maximum possible extension of ~8.70 nm of the overall system. This indicates that the overall shape of AuDLC* could be best described as a flat ellipsoid, directed by the packing requirements of the rigid discogens. AuDLC* can thus be viewed as a macrodisk (Fig. 2b); this is distinctly different to the shape of calamitic functionalized NPs which are often viewed as sphero-cylinders. In other words, for the investigated system the shape of the corona replicates to some extend the shape of the mesogens.

The formation of the macroscopic N_D^* phase of the mesogens of the column forming AuNPs is due to the long flexible alkyl spacer, decoupling mesogens from the NP cores. As a result, even at high levels of surface coverage; no steric crowding occurs; orientational mobility is maintained. This is different for shorter spacer lengths of discogen ligands as evidenced in the results for a non-chiral system where no superstructure was detected.[20] As the lattice parameters change very little with temperature this supports the view that the N_D^* helix is perpendicular to the base of the lattice; characterized by only orientational ordering of the system; similar to other chiral materials.[17]

To characterize the chirality further, series of CD spectra as a function of temperature for the nanocomposite AuDLC* and the free chiral discogen in thin films were recorded over a range of temperatures. For AuDLC* (Fig. S11a and b†), the largest increase in ellipticity at 460 nm on cooling is between 95 °C and 90 °C. This corresponds to the isotropic-N_D^* transition, and for the free ligand (Fig. S11c†) this occurs at 95 °C. To systematically exclude the contribution of the birefringence to the signal

of the LC phase, samples were sheared in the preparation of a quartz cell before CD experiments. The LC domains were found to be small and numerous after shearing, thus the contributions from linear dichroism and birefringence are expected to cancel out. This hypothesis was confirmed by rotating the sheared sample in an interval of 90° (Fig. S11d†) and additionally turning the sample over; only small changes in value but not in the sign of the CD signal occurred.[17]

The CD bands in the UV region for AuDLC* are linked to the helical arrangement of ligands attached to AuNPs. On further cooling to 70 °C (Fig. 1f and S13†), an increase of the positive CD signal in the wavelength region of 355–437 nm occurred as well as a negative signal in the plasmonic region of the gold core (Fig. S11b†) (around 520 nm at 70 °C) appears. This plasmonic signal fluctuated in value on cooling further. The consistently negative value of this CD signal is in line with a tangential dipole of the attached organic corona.[29,30] On further cooling, between 60 °C and 55 °C (see Fig. S12b and S13†), an enhancement of the negative signal at 325 nm was observed. We associate these processes with an increased twisting of the mesogenic structures in the chiral nematic. We see fundamentally two processes, the first is associated with N_D^* phase formation from the isotropic liquid, associated with the increased chiral distortions of the organic corona. The second process, commencing at ~70 °C, is linked to chiral interactions of the NPs. Here, the packing distance measured by the lattice parameter b (2.52 nm), similar to the NP diameter (2.5 ± 0.5 nm) is the primary candidate. In the $p2$ lattice, the position of the gold cores along the axis c perpendicular to the lattice plane is not defined (see Fig. 2a).

Due to size variation and NPs being out of position (translated along c), some disordering exists and this leads to formation of a $p2$ lattice by time and space averaging. On cooling the system contracts along the third dimension c and the proximity of the gold cores enveloped by a chiral surface increases. As the CD signal is small in value, when compared to theoretical models, this suggests short range ordering is developed.[31]

To reconcile XRD, POM, DSC and CD data we propose a model which is schematically shown in Fig. 2. To minimize energy and to enhance attractive van der Waals interactions of the mesogens, the particles form an overall elongated ellipsoid shape with the mesogens at the periphery and the gold cores at the centre (Fig. 2b); determined by the volume content of the NPs, their size and size distribution a columnar superstructure of the NPs is formed, similar to other systems.[32] In this model, the chiral centers at the gold surface form a chiral envelope (green corona). On entering the N_D^* phase a chiral nematic helix orthogonal to the lattice plane is formed (Fig. 2c). With lowering the temperature, the CD signal in the plasmonic region of the NPs; indicative an additional helical structure along the axis of the smallest lattice parameter, as schematically shown in Fig. 2d is detected. Small translations of the system parallel to the main axis of the mesogens and packing requirements decreasing the overall volume with lower temperature are responsible for this. This is in accord with results for other chiral coated surfaces in assemblies.[33,34] The CD signals in the UV region are associated with the changing chiral environment of the mesogens. The signals in the plasmonic region are through the interactions of the gold NPs.

Conclusions

In summary, we have demonstrated that it is possible to obtain a thermodynamically stable chiral discotic nematic phase from undiluted NPs coated with a chiral discogen. To pack efficiently into a superlattice, detected by SXRD, the organic corona of the NPs takes the shape of a macrodisk. On entering the LC phase SRCD in thin films shows a chiral signal associated with the discotic chiral nematic phase, at lower temperatures a second process linked to a chiral association behaviour of the NPs can be detected. This approach opens up the route towards plasmonic high load nanocomposites where plasmonic chirality can be engineered by addressing the interactions of the organic LC phase forming corona.

Conflicts of interest

There are no conflicts to declare.

Acknowledgements

H. Y. thanks the China Scholarship Council (CSC) for a doctoral scholarship. This work was supported by the National Natural Science Foundation of China (No. 21774099) and the Science and Technology Agency of Shaanxi Province (2016KW-050 and 2018KWZ-03). The authors thank for the support by the 111 Project 2.0 (BP2018008). We also thank Dr G. Siligardi, Dr R. Hussain and Dr T. Jávorfi for the beamline test at B23 Diamond Light Source and staff at beamline BL16B1 at Shanghai Synchrotron Radiation Facility.

Notes and references

1 S. Bhattacharjee, M. I. Khan, X. Li, Q. Zhu and X. Wu, *Catalysts*, 2018, **8**, 120.
2 J. T. Collins, C. Kuppe, D. C. Hooper, C. Sibilia, M. Centini and V. K. Valev, *Adv. Opt. Mater.*, 2017, **5**, 1700182.
3 T. Yasukawa, H. Miyamura and S. Kobayashi, *Chem. Soc. Rev.*, 2014, **43**, 1450–1461.
4 L. Cseh and G. H. Mehl, *J. Am. Chem. Soc.*, 2006, **128**, 13376–13377.
5 H. Qi and T. Hegmann, *J. Mater. Chem.*, 2006, **16**, 4197–4205.
6 V. Caligiuri, L. De Sio, L. Petti, R. Capasso, M. Rippa, M. G. Maglione, N. Tabiryan and C. Umeton, *Adv. Opt. Mater.*, 2014, **2**, 950–955.
7 A. Nemati, S. Shadpour, L. Querciagrossa, L. Li, T. Mori, M. Gao, C. Zannoni and T. Hegmann, *Nat. Commun.*, 2018, **9**, 1–13.
8 M. Mitov, C. Portet, C. Bourgerette, E. Snoeck and M. Verelst, *Nat. Mater.*, 2002, **1**, 229–231.
9 J. S. Pendery, O. Merchiers, D. Coursault, J. Grand, H. Ayeb, R. Greget, B. Donnio, J. Gallani, C. Rosenblatt, N. Félidj,

Y. Borenszteinab and E. Lacaze, *Soft Matter*, 2013, **9**, 9366–9375.
10 L. Wang, H. Dong, Y. Li, C. Xue, L. Sun, C. Yan and Q. Li, *J. Am. Chem. Soc.*, 2014, **136**, 4480–4483.
11 S. Shadpour, J. P. Vanegas, A. Nemati and T. Hegmann, *ACS Omega*, 2019, **4**, 1662–1668.
12 R. Singh, K. N. Unni and A. Solanki, *Opt. Mater.*, 2012, **34**, 716–723.
13 R. Farshchi, M. Ramsteiner, J. Herfort, A. Tahraoui and H. T. Grahn, *Appl. Phys. Lett.*, 2011, **98**, 162508.
14 J. F. Sherson, H. Krauter, R. K. Olsson, B. Julsgaard, K. Hammerer, I. Cirac and E. S. Polzik, *Nature*, 2006, **443**, 557–560.
15 G. L. R. Greget, C. Dominguez, Z. T. Nagy, D. Guillon, J. L. Gallani and B. Donnio, *Beilstein J. Org. Chem.*, 2012, **8**, 349–370.
16 L. Cseh and G. H. Mehl, *J. Mater. Chem.*, 2007, **17**, 311–315.
17 L. Cseh, X. Mang, X. Zeng, F. Liu, G. H. Mehl, G. Ungar and G. Siligardi, *J. Am. Chem. Soc.*, 2015, **137**, 12736–12739.
18 L. C. Henderson, J. M. Altimari, G. Dyson, L. Servinis, B. Niranjan and G. P. Risbridger, *Bioorg. Chem.*, 2012, **40**, 1–5.
19 L. Đorđević, F. Arcudi, A. D'Urso, M. Cacioppo, N. Micali, T. Bürgi, R. Purrello and M. Prato, *Nat. Commun.*, 2018, **9**, 1–8.
20 M. Gupta, S. S. Mohapatra, S. Dhara and S. K. Pal, *J. Mater. Chem. C*, 2018, **6**, 2303–2310.
21 F. Vera, J. L. Serrano and T. Sierra, *Chem. Soc. Rev.*, 2009, **38**, 781–796.
22 J. Malthéte and A. Collet, *J. Am. Chem. Soc.*, 1987, **109**, 7544–7545.
23 M. A. Shcherbina, X. B. Zeng, T. Tadjiev, G. Ungar, S. H. Eichhorn, K. E. S. Phillips and T. J. Katz, *Angew. Chem., Int. Ed.*, 2009, **48**, 7837–7840.
24 M. Brust, M. Walker, D. Bethell, D. J. Schiffrin and R. Whyman, *J. Chem. Soc., Chem. Commun.*, 1994, **7**, 801–802.
25 J. Dintinger, B. J. Tang, X. Zeng, F. Liu, T. Kienzler, G. H. Mehl, G. Ungar, C. Rockstuhl and T. Scharf, *Adv. Mater.*, 2013, **25**, 1999–2004.
26 X. Zeng, F. Liu, A. G. Fowler, G. Ungar, L. Cseh and G. H. Mehl, *Adv. Mater.*, 2009, **21**, 1746–1750.
27 D. V. Leff, P. C. Ohara, J. R. Heath and W. M. Gelbart, *J. Phys. Chem.*, 1995, **99**, 7036–7041.
28 M. J. Hostetler, J. E. Wingate, C.-J. Zhong, J. E. Harris, R. W. Vachet, M. R. Clark, J. D. Londono, S. J. Green, J. J. Stokes, G. D. Wignall, G. L. Glish, M. D. Porter, N. D. Evans and R. W. Murray, *Langmuir*, 1998, **14**, 17–30.
29 X. Wang and Z. Tang, *Small*, 2017, **13**, 1601115.
30 A. O. Govorov and Z. Fan, *ChemPhysChem*, 2012, **13**, 2551–2560.
31 J. Kumar, K. G. Thomas and L. M. Liz-Marzán, *Chem. Commun.*, 2016, **52**, 12555–12569.
32 Z. Fan and A. O. Gavorov, *J. Phys. Chem. C*, 2011, **115**, 13254–13261.
33 H. Kang, J. T. Buchman, R. S. Rodriguez, H. L. Ring, J. He, K. C. Bantz and C. L. Haynes, *Chem. Rev.*, 2019, **119**, 664–699.
34 S. Mokashi-Punekar, Y. Zhou, S. C. Brooks and N. L. Rosi, *Adv. Mater.*, 2019, 1905975.